EPJ Photovoltaics **16**, 15 (2025)
© M. Mehler et al., Published by EDP Sciences, 2025
https://doi.org/10.1051/epjpv/2025006

Available online at:
www.epj-pv.org

Special Issue on 'EU PVSEC 2024: State of the Art and Developments in Photovoltaics', edited by Robert Kenny and Gabriele Eder

ORIGINAL ARTICLE OPEN ACCESS

Impact of high-temperature processing steps on the long-term stability of charge carrier lifetime in *n*-type FZ-silicon

Melanie Mehler[1,*], Nicolas Weinert[1], Nicole Aßmann[2], Axel Herguth[1], Giso Hahn[1], and Fabian Geml[1]

[1] University of Konstanz, Department of Physics, 78457 Konstanz, Germany
[2] Centre for Materials Science and Nanotechnology, University of Oslo, N-0371 Oslo, Norway

Received: 9 July 2024 / Accepted: 28 January 2025

Abstract. In this work, the long-term behavior of excess charge carrier lifetime in *n*-type FZ-Si wafers without presence of highly doped layers is investigated during illumination at elevated temperatures. Thereby, the influence of high-temperature processing steps such as short high temperature thermal treatment, often referred to as tabula rasa (TR), and phosphorus diffusion gettering is considered. Degradation of effective lifetime is observed as well as a very strong regeneration effect that significantly exceeds the initial effective lifetime value. The phosphorus gettering step appears to have no significant effect on the degradation and regeneration behavior. Samples subjected to a TR treatment show only bulk-related regeneration. Investigations in darkness showed that the bulk-related regeneration is carrier-induced and not necessarily light-induced. FT-IR measurements at 5 K showed that the samples with a TR step have a higher O_i concentration in the Si bulk and that the hydrogen-passivated vacancies (VH_4) are dissolved. The regeneration behavior of the samples with a TR step could be correlated with a reduced vacancy concentration. Such a thermal processing step appears to offer a strong mitigation strategy.

Keywords: Long-term stability / *n*-type / FZ-Si / thermal anneal / oxygen / point defects

1 Introduction

In recent years, significant progress has been made in the development of solar cell concepts using *n*-type silicon (Si) wafers enabling solar cells with higher efficiency potential, e.g. tunnel oxide passivating contacts (TOPCon). These solar cell concepts involve high-temperature steps during cell processing, which can affect the defect structure of the Si wafers. High-temperature steps such as boron/phosphorous diffusion and thermal oxidation can result in the formation of silicon oxide precipitates (or agglomerates) from small clusters of interstitial oxygen (O_i) interacting with vacancies and their agglomerates [1]. Since silicon oxide agglomerates can act as recombination centers and internal gettering sites [2], the efficiency of the resulting cell can be affected [3,4]. A short high-temperature annealing step ≥1050 °C, known as tabula rasa (TR) [5], can dissolve the silicon oxide agglomerates and nucleation sites [6]. The dissolution of silicon oxide agglomerate nuclei during TR can lead to an improvement of bulk minority charge carrier lifetime τ_{bulk} [7].

Apart from the effect on the dissolution of silicon oxide agglomerates, a TR step can lead to formation of Si vacancies and self-interstitials (Frenkel pairs) [1]. Both species are fairly mobile at high temperatures, but due to different diffusivities ($D_I \sim 10^{-4}\,cm^2/s$ [8] vs. $D_v \sim 10^{-5}\,cm^2/s$ [8,9]), more interstitials than vacancies reach the surface and annihilate there resulting in a rather vacancy-rich bulk. If, however, TR takes place in an oxidizing ambient and a SiO_2 layer grows, interstitials are released at the surface [10,11] that flood the bulk and annihilate there with vacancies resulting in a vacancy-lean bulk [12,13]. Subsequent rapid cooling of the Si wafers suppresses the formation of new Frenkel pairs and freezes the imbalance of intrinsic defects. It has been shown that the TR process can mitigate the process-induced degradation effect in *n*-type Czochralski (Cz)-Si wafers [1] and that the carrier lifetime degradation might be related to intrinsic defects (vacancies, interstitials, and their aggregates) [1,14]. According to Ochoa et al. [14], the carrier lifetime degradation after a TR process in N_2 can be attributed to the formation of Si vacancy defects.

Degradation phenomena such as light and elevated temperature induced degradation (LeTID) can significantly reduce the bulk excess charge carrier lifetime and thereby affect the efficiency of solar cells. Although the root cause of LeTID is not fully understood yet, several influencing factors

* e-mail: melanie.mehler@uni-konstanz.de

This is an Open Access article distributed under the terms of the Creative Commons Attribution License (https://creativecommons.org/licenses/by/4.0), which permits unrestricted use, distribution, and reproduction in any medium, provided the original work is properly cited.

have been found in p-type Si materials. It could be shown that LeTID strength and kinetics depend on various parameters such as the temperature during the degradation investigation [15,16], excess charge carrier concentration (or injection) [15] and hydrogen (H) content after in-diffusion from passivation layers [17–19]. Meyer et al. [20] propose that the defect responsible for LeTID in p-type Cz-Si may be attributed to the presence of Si vacancies. Although LeTID has mainly been studied in p-type Si, recent studies have shown that LeTID can also occur in n-type mc- and Cz-Si materials [21–24], in the presence of a highly doped region, mostly p^+. Degradation and regeneration were also observed in non-diffused n-type FZ-Si wafers with a base resistance of ~1.6 Ωcm [25]. The study also highlighted the effect of SiN_x deposition temperature, showing that degradation occurred following a deposition at 650 °C, but was not observed at lower deposition temperatures of 100 °C or 300 °C.

In order to gain a deeper insight into the long-term stability on n-type Si wafers without presence of a highly doped layer, the influence of high-temperature processing steps, such as TR and/or gettering, on the degradation and regeneration behavior is investigated here. To investigate the impact of high-temperature steps on the defect structure of the Si-bulk directly after firing, Fourier transform infrared (FT-IR) spectroscopy measurements are performed at low temperature to analyze the change in concentration of interstitial oxygen and vacancy-hydrogen bonds.

2 Experimental

For the long-term stability experiments, 250 µm thick n-type phosphorus-doped float-zone (FZ)-Si wafers with base resistivity of ~2.3 Ωcm were used as base material. FZ-Si material was chosen because FZ wafers contain minimal impurities and defects, making them ideal for isolating the impact of thermal processes on degradation mechanisms. Figure 1 shows the process flow diagram for the differently processed n-type FZ-Si wafers. For each group, a complete FZ-Si wafer was used and subsequently divided into 5×5 cm^2 pieces. To ensure consistent defect distributions, the lifetime tests were conducted on samples taken from identical positions on the wafers. After an HF etching step to remove any surface oxide, the samples, except for a reference group, underwent either a TR step, a phosphorus gettering step (G) or a combination of both (TR+G). Here, the TR processing step for FZ-Si is performed at 1050 °C for 30 min in O_2 atmosphere. After a subsequent HF etching step, TR+G and G samples were gettered using a $POCl_3$ diffusion at 837 °C. All samples were then KOH etched to remove the resulting emitter and to achieve the same thickness, ensuring the same temperature profile during the simulated contact firing process for all samples. After a cleaning step, all samples received on the front and back side a 75 nm SiN_x:H layer by plasma-enhanced chemical vapor deposition (PECVD) as surface passivation. The samples were then fired in a belt furnace at a measured sample peak temperature of $T_{peak} = 800$ °C.

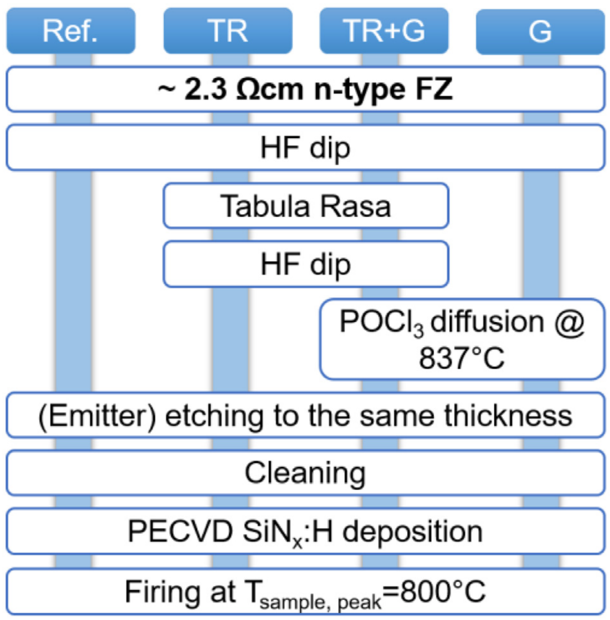

Fig. 1. Schematic process flow diagram for the differently processed n-type FZ-Si samples, which are divided into four groups. Except for the reference group (Ref.), the samples underwent either a TR-step (TR), a phosphorus gettering step (G) or a combination of both (TR+G).

The effective minority charge carrier lifetime τ_{eff} was determined using the photoconductance decay (PCD) method (WCT-120 from Sinton Instruments) at 30 °C and evaluated at an injection level of $\Delta n = 0.1\ n_0 = 2 \cdot 10^{14}$ cm^{-3}, with n_0 being the doping density. From the resulting PCD measurements, the change in lifetime equivalent defect density ΔN_{leq} is calculated via

$$\Delta N_{leq} = \frac{1}{\tau_{eff,t}} - \frac{1}{\tau_{eff,0}} \propto \Delta N_{SRH} \quad (1)$$

with $\tau_{eff,0}$ and $\tau_{eff,t}$ being the effective lifetime directly after the final high-temperature step and at any given time, respectively [26]. The change in lifetime equivalent defect density ΔN_{leq} is proportional to the change in defect density of the Shockley-Read-Hall (SRH) defects and can be either positive or negative, depending on whether recombination-active defects are formed or dissolved during the treatment process. In addition to determination of ΔN_{leq}, the PCD measurements were also used to evaluate the changes in surface-related saturation current density Δj_0 through difference analysis as described in [27]. The samples were treated at a constant illumination of 0.9 ± 0.1 sun photon flux equivalent, while being heated to a temperature of 100 °C on a hotplate. To assess the long-term stability in the absence of light, identically processed samples were degraded in the dark at a temperature of 100 °C.

In addition to the lifetime measurements, FT-IR measurements at 5 K were conducted using a Bruker IFS 125HR spectrometer equipped with a KBr beam splitter in the mid-infrared range. The sample preparation for the FT-IR measurements is based on the concept presented in

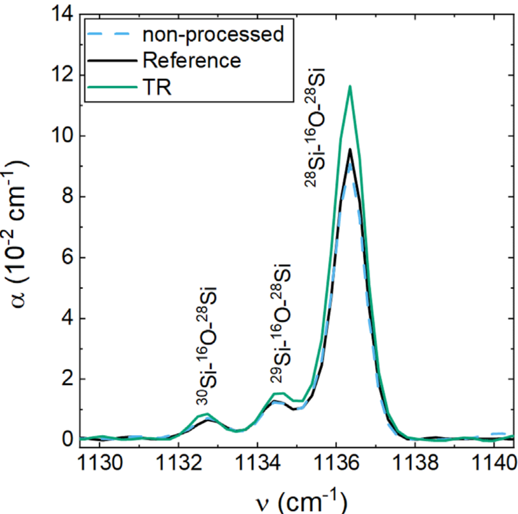

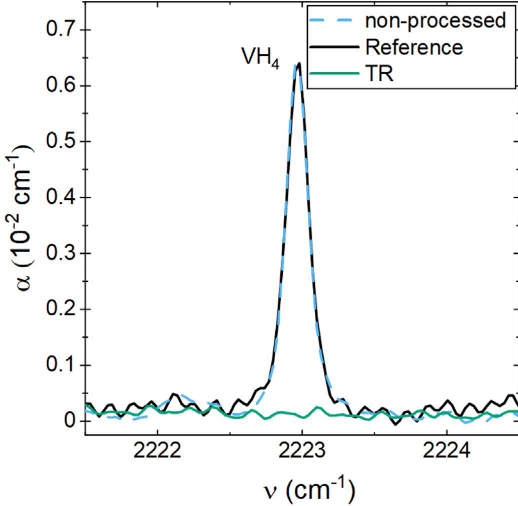

Fig. 2. IR absorption coefficient spectra of O_i (left) at 1132-1138 cm^{-1} and of VH_4 (right) at 2223 cm^{-1} for differently processed *n*-type FZ-Si samples. Additionally, a non-processed *n*-type FZ-Si sample is used as a comparison alongside the processed and fired reference sample. Since the two reference curves overlap, the line of the as-cut reference sample is dashed for better visualization.

[28]. After firing the *n*-type FZ samples at $T_{peak} = 800\,°C$, the wafers were cleaved into pieces of $10\times10\ mm^2$. These pieces were stacked to form a cuboid of $10\times10\times5\,mm^3$, resulting in an absorption path length of 10 mm and a maximal cross section of 5 mm. A liquid nitrogen-cooled mercury cadmium telluride (MCT) detector was used for the FT-IR measurement of interstitial oxygen and a liquid nitrogen-cooled indium antimony (InSb) detector was used for the measurement of the vacancy-hydrogen bonds.

3 Results and discussions

3.1 FT-IR measurements

Despite the rather low concentration of oxygen in FZ-Si we were able to identify the local vibration mode (LVM) of interstitial oxygen O_i by FT-IR. Figure 2 (left) shows the absorption coefficient spectra in the region of the O_i LVM for the differently processed samples. In addition to the processed and fired reference sample, a non-processed (out of the box) *n*-type FZ wafer serves as comparison. The FT-IR measurements show three peaks for O_i, with the measured O_i peaks being higher for the sample with a TR step compared to the references. To determine the O_i concentration in the Si bulk, the total area of the peaks is calculated and multiplied by the calibration factor $AO_i = (9.6 \pm 0.1) \cdot 10^{15}\,cm^{-1}$ [29]. The concentrations directly after firing are found to be $[O_i] = (13.6 \pm 0.2) \cdot 10^{14}\,cm^{-3}$ for the sample with a TR step, $[O_i] = (10.5 \pm 0.2) \cdot 10^{14}\,cm^{-3}$ for the 'out of the box' (non-processed) sample, and $[O_i] = (10.9 \pm 0.2) \cdot 10^{14}\,cm^{-3}$ for the processed reference sample. As expected, the sample with a TR step exhibits a higher O_i concentration compared to the samples without this step, which can be attributed to the dissolution of silicon oxide agglomerates during the TR step. In contrast, there are only minimal differences between the references in $[O_i]$ indicating that the firing step does not impact $[O_i]$ significantly.

The LVM of the vacancy-hydrogen defect VH_4, consisting of a single vacancy with four hydrogen atoms, could be detected at 2223 cm^{-1} [30] as well as shown in Figure 2 (right). In many theoretical and experimental studies, models for vacancy-hydrogen (VH_n with $n = 1,2,3,4$) defects were developed [30–35]. As the number of hydrogen atoms increases, the Si-H bonds shorten due to the mutual repulsion of the hydrogen atoms, leading to an increase in the frequencies of the local Si-H vibrational modes [30]. Consequently, the LVM frequencies of VH_4 are the highest of all VH_n defects. Unfortunately, no FT-IR calibration factor for VH_4 is known to us, hence, the actual concentration $[VH_4]$ could not be calculated from Figure 2 (right). In [36] the vacancy concentration in the center of a FZ wafer was determined to be approximately $10^{14}\,cm^{-3}$ by measuring the concentration of rapidly diffusing elements such as platinum and gold, which occupy silicon vacancies, hence, the observed VH_4 absorption peak for the (non)-processed sample might correspond to such a concentration but it is unclear whether our FZ sample is comparable to the one used in [36]. In contrast to the processed reference sample and the 'out of the box' sample, the LVM of VH_4 could not be detected in the sample with a TR step. Based on the findings in [29], VH_4 in proton-implanted silicon starts to anneal out near 530 °C. It is thus likely that hydrogen is released from the vacancies at such high temperatures applied for the TR step and probably effuses from the sample. In parallel as mentioned above, the high temperatures during the TR step in O_2 ambient flooding the bulk with interstitials enable the recombination of (then hydrogen-free) vacancies and interstitial atoms, reducing the number of vacancies. Hence, even though the sample is flooded with hydrogen during the subsequent firing step, significantly fewer VH_4 complexes may form, confirming the studies that assume that a TR step reduces the number of vacancies [1,37]. Since the processed reference sample shows almost no difference in VH_4 compared to the non-processed sample, VH_4 probably

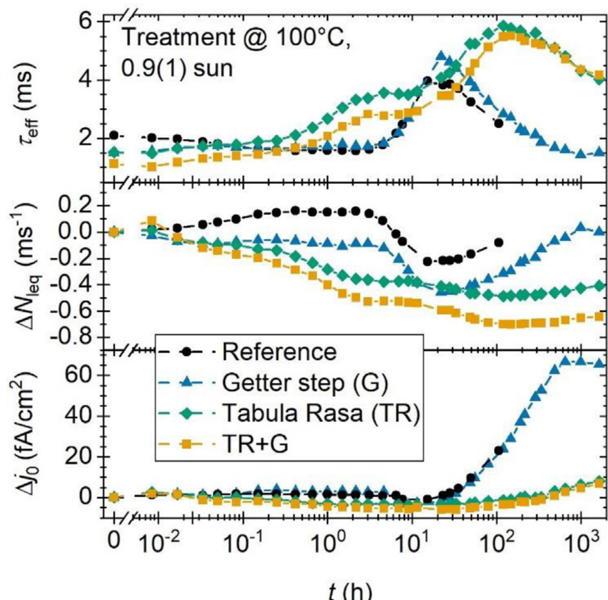

Fig. 3. Effective lifetime τ_{eff} (top), lifetime equivalent defect density ΔN_{leq} (middle) and change in surface-related saturation density Δj_0 (bottom) versus accumulated treatment time for differently processed n-type FZ samples. Samples were degraded at 0.9(1)suns photon flux equivalent and a temperature of 100 °C. The lines in the graphs are guide-to-the-eye.

also dissolves (partly) during firing but forms again during the cooling process. Another possible explanation might be that the firing process is quite fast, with the samples being at T_{peak} >700 °C for only a few seconds, leading to negligible changes.

3.2 Lifetime measurements

Figure 3 shows τ_{eff}, ΔN_{leq} and Δj_0 over accumulated time for the differently processed n-type FZ-Si wafers fired at T_{peak} = 800 °C. The reference sample, which was not subjected to high-temperature treatment before firing, shows a slight degradation in τ_{eff} from ~2 ms to ~1.5 ms within the first 2 h, followed by a strong regeneration in τ_{eff} from ~1.5 ms to ~4 ms, consistent with our previous findings [38]. After regeneration, τ_{eff} shows a renewed degradation from 15 h onwards, which can be attributed to a decreasing surface passivation quality (steady increase of Δj_0). Compared to the reference sample, the gettered sample shows almost the same degradation and regeneration behavior. In contrast, the samples that have undergone a TR step show no degradation, but a two-step regeneration. Overall τ_{eff} increases from ~1 ms up to ~6 ms within the first 100 h. The Δj_0 values show a slight decrease up to 6 fA/cm^2 during the two-stage regeneration, which will be discussed later. After 100 h treatment time the samples with a TR step show a decrease in τ_{eff}. Because of the steady increase of Δj_0, the degradation can be attributed to surface-related degradation.

The samples TR and TR+G do not show a significant difference in degradation and regeneration behavior. The initial lifetime of the differently processed samples is less than 2 ms, which is relatively low for FZ-Si. A possible reason for this low initial lifetime and the weaker degradation compared to the stronger regeneration might be that degradation had already begun during the firing process, leading to pre-existing defects in the samples. This assumption is supported by the findings of Niewelt et al. [39], who demonstrated that the photoluminescence images of n-type samples immediately after firing display a similar pattern to those of degraded p-type samples. The absolute j_0-values immediately after firing were found to be 7.8 fA/cm^2 for the reference, 6.9 fA/cm^2 for the gettered sample, 8.1 fA/cm^2 for the sample with a TR step, and 8.4 fA/cm^2 for the samples with TR+G, determined using the Kimmerle method [40]. The initial τ_{eff} values do not seem to be directly linked to the slightly varying surface passivation quality.

To investigate whether the effect is light-induced, the study was also performed on identically processed samples in the dark. Figure 4 shows τ_{eff}, ΔN_{leq} and Δj_0 over accumulated time for identically processed n-type FZ-Si wafers as for the experiment under illumination, fired at T_{peak} = 800 °C and annealed at 100 °C in the dark. The reference sample initially shows a slight improvement in lifetime. After ~2 min, degradation begins and reaches its maximum after ~7 h. Beyond this point, the lifetime remains relatively stable. When compared to the reference sample degraded under illumination, see Figure 3, it can be seen that there is no significant regeneration within 1000 h at 100 °C. Only after increasing the temperature at 180 °C the sample shows significant regeneration up to 5 ms, followed by significant degradation, again caused by degradation of surface passivation quality (increasing j_0).

Similar to the investigation under illumination, the samples with a TR step show no bulk-related degradation, but regeneration. During the first 10 h of treatment, the lifetimes of the TR and TR+G samples remain relatively stable, with a slight tendency towards improvement. After this period, regeneration is more pronounced in both samples. The sample with a TR step shows an increase in τ_{eff} from ~1 ms to ~3 ms after 1000 h treatment time, while the sample with a TR+G step shows an increase from ~1 ms to ~6 ms. In order to accelerate the kinetics, the temperature of the hotplate was increased to 180 °C after 1000 h, resulting in additional slight improvement after 1000 h. Again, during the regeneration phase, τ_{eff} values higher than the initial value are achieved. The samples treated under illumination (Fig. 3) exhibit two regeneration phases: the first occurring at 1 h and the second at 10 h. Under dark conditions two regeneration steps can also be recognized for the TR and TR+G samples: the first at 10 h and the other at 100 h. Since the regeneration kinetics are accelerated under illumination, the effect therefore appears to be charge carrier-induced. While the Δj_0 values of the sample with the TR+G treatment remain almost constant, Δj_0 values of the sample with only the TR step decrease 45 h after the hotplate temperature is increased. The absolute j_0-values immediately after firing were found to be 10 fA/cm^2 for the reference, 13.3 fA/cm^2 for the sample with a TR step

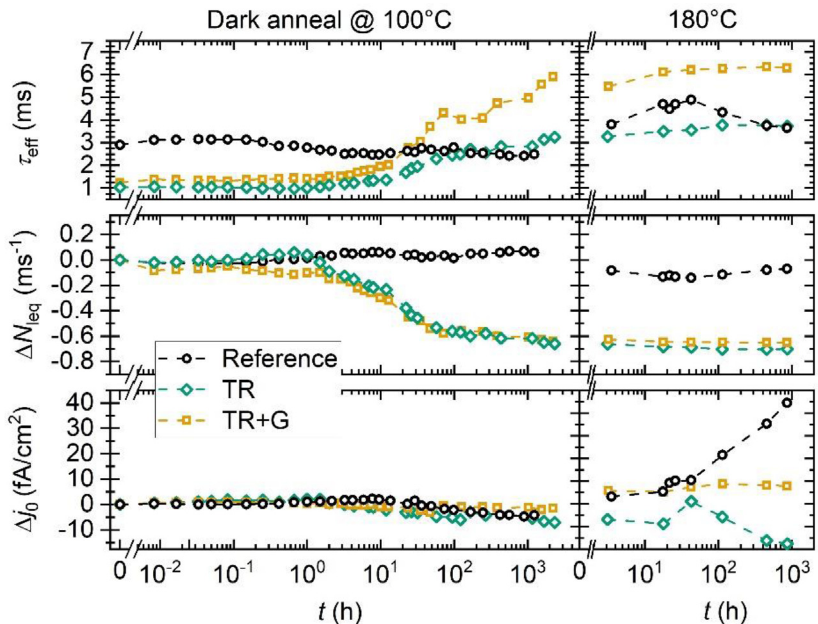

Fig. 4. Effective lifetime τ_{eff} (top), lifetime equivalent defect density ΔN_{leq} (middle) and change in saturation density Δj_0 (bottom) versus accumulated treatment time for differently processed *n*-type FZ samples. Samples were degraded at 100 °C in the dark. After 1000 h, the treatment temperature is increased to 180 °C. The lines in the graphs are guide-to-the-eye.

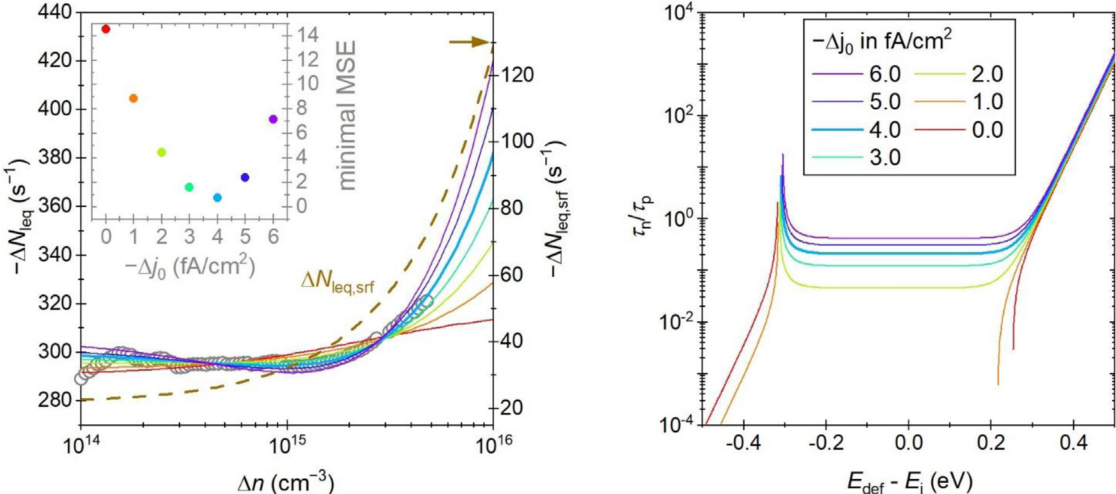

Fig. 5. (Left): Injection-dependent (negative) lifetime equivalent defect density ΔN_{leq} of the TR sample from Figure 3 at 1 h (compared to 0 h) and best matching SRH fit curves assuming different improvements in surface passivation quality given as (negative) Δj_0. The 4.0 fA/cm^2 curve corresponds to the minimal overall MSE (shown in the inset). The dashed line shows the contribution of the changed surface passivation quality to overall ΔN_{leq}. (Right): Results of the SRH parameter surface analysis showing the combinations of τ_n/τ_p and energy level E_{def} (relative to the intrinsic Fermi level E_i lying close to mid-gap) that result in the lowest mean square error for the ΔN_{leq} (Δn) data from Figure 5 (left) assuming different improvements in surface passivation quality given by (negative) Δj_0. The light blue 4.0 fA/cm^2 curve corresponds to the minimum overall MSE.

and 8.2 fA/cm^2 for the samples with TR+G. Although the j_0-value for the TR+G sample is lower than that of the other two samples, the sample does not exhibit a higher initial lifetime, indicating that defects in the Si bulk are already present after firing.

The regeneration behavior of the samples with TR step can be attributed to a deactivation or dissolution of defects in the Si bulk. Niewelt et al. [39] also observed only an improvement of τ_{eff} under LeTID conditions (75 °C, 1 sun equivalent illumination) in non-diffused *n*-type FZ material. In their study, the samples were pre-treated with an oxidation at 1050 °C and subsequently passivated with an AlO_x/SiN_x:H layer. They suggest that the significant increase in τ_{eff} is caused by the deactivation of bulk defects that are already present after firing. Since no VH_4 could be measured in the samples with a TR step and the silicon oxide

agglomerates dissolved, the deactivation or dissolution of the defects, responsible for the regeneration effect, does not appear to be directly caused by these vacancies and/or silicon oxide agglomerates configurations. But note that although no VH_4 was detectable in the samples with a TR step, there could still be vacancies in the Si bulk that are either in an infrared inactive configuration or whose concentration is below the detection limit of FT-IR. Assuming that bulk defects, such as vacancies, are responsible for the degradation, which Meyer et al. [20] suggest, one would expect a higher lifetime directly after firing for the samples including a TR step, which does not seem to be the case (Fig. 3 top and Fig. 4 top). Therefore, the vacancy concentration alone might not be the decisive factor for the amount of defects formed directly after firing. But the lifetime in the regenerated state is higher for the samples with TR (with lower vacancy concentration). The maximum lifetime of the regenerated state might therefore be related to the vacancy concentration.

To get a deeper insight into the defect during regeneration, the injection-resolved defect density ΔN_{leq}, exemplarily for the TR sample from Figure 3 at 1 h (compared to 0 h) shown in Figure 5 (left), is investigated in more detail. Note that ΔN_{leq} is in fact negative indicating a loss of defects, however, for reasons of compatibility with other studies typically focussed on defect formation, Figure 5 (left) shows $-\Delta N_{\mathrm{leq}}$ instead meaning a reversal of time and thus an apparent formation of defects (see Eq. (1)).

In the work of Herguth [26], the injection dependence of ΔN_{leq} for deep- and shallow-level SRH bulk defects during defect formation is exemplary described for p-type Si. It is shown that for deep SRH defects, ΔN_{leq} always decreases with increasing injection levels, while for shallow defects, ΔN_{leq} exhibits in most cases the opposite behavior, an increase as injection levels rise. In both cases, the curve shape is sigmoidal, either up- or downward bent, when plotted on a logarithmic Δn scale. Whether a defect appears as a rather deep or rather shallow defect in SRH theory depends on the position of its defect level E_{def} relative to the intrinsic Fermi level E_{i} (located close to mid-gap) and there is a certain transition region in between. Herguth [26] also introduces a surface related defect density $\Delta N_{\mathrm{leq,srf}}$ resulting from a deterioration of surface passivation quality indicated by an increase in j_0. This $\Delta N_{\mathrm{leq,srf}}$ exhibits an increasing trend with injection and may (due to a limited Δn range) be confused with a shallow SRH bulk defect even though it features a different injection dependence: $\Delta N_{\mathrm{leq,srf}} \propto (n_0 + \Delta n) \cdot \Delta j_0$. Note that this corresponds to an exponential increase when plotted on a logarithmic Δn scale.

At first glance, $-\Delta N_{\mathrm{leq}}$ in Figure 5 (left) shows an increasing trend with Δn suggesting either a shallow SRH bulk defect or a change in surface passivation quality. Using the SRH parameter surface approach proposed elsewhere [41], the best fit parameters of a potential SRH bulk defect where detemined and Figure 5 (right) shows the correpending $\tau_{\mathrm{n}}/\tau_{\mathrm{p}}$ ratio for parameter combinations that minimze the mean squared error (MSE). In a first attempt, a potential change in surface passivation quality was rejected ($\Delta j_0 = 0$, red lines). The best solution is then a shallow SRH bulk defect whose energy level is located either close to the valence or conduction band with a wide range of possible $\tau_{\mathrm{n}}/\tau_{\mathrm{p}}$ values. However, the best curve fitted with $\Delta j_0 = 0$ in Figure 5 (left, red line) does not reproduce the increase towards higher injection visible in the experimental data resulting in a rather high minimum MSE (inset of Fig. 5 (left)). Hence, the SRH fitting procedure was repeated now including an improvement in passivation quality corresponding to negative Δj_0 values. Indeed, the curves are then stronger upwards-bent towards higher injection and there is an optimum for the minimum MSE at -4.0 fA/cm^2 (inset of Fig. 5 (left)). Figure 5 (left) also shows the contribution of the surface to ΔN_{leq} in this optimum (dashed line) indicating also that the observed data cannot be explained by a change in surface quality alone but requires an additional change in bulk defect density as well. However, a look on Figure 5 (right) shows that this defect is not neccesarily a shallow SRH bulk defect. It can be either a deep defect with an energy level close to mid-gap exhibiting a fixed $\tau_{\mathrm{n}}/\tau_{\mathrm{p}}$ ratio of ~0.15 or a shallow defect with an energy level close to the conduction band with a wide range of possible $\tau_{\mathrm{n}}/\tau_{\mathrm{p}}$ values. The reason behind this change can be best seen in the 6.0 fA/cm^2 curve (violet line) which is already beyond the MSE optimum. With such a high value, the $\Delta N_{\mathrm{leq,srf}}$ curve is strongly bent upwards towards higher injection, hence, a potential bulk defect has to compensate this upward trend at high injection with a corresponding downward trend which is characteristic for a deep SRH defect. However, this downward trend continues to lower injection as well where the surface contribution is only weakly injection-dependent. Consequently, a minimum is formed where the surface related upward and the bulk related downward trend compensate each other. Such a minimum might be present in the experimental data but cannot be taken as granted in view of the variations.

In summary, it is likely that the regeneration of the TR sample in Figure 3 can be attributed to two different effects. On the one hand, the surface passivation quality improves, likely by 4.0 fA/cm^2. However, this improvement alone cannot consistently explain the observed extent of improvement and injection dependence of ΔN_{leq}. On the other hand, a SRH bulk defect seems to disappear which is either a deep level defect or a shallow defect close to the conduction band. The analysis at different times not discussed here in detail shows that the surface improvement occurs early in the measurement series while the disappearance of bulk defects continues at least until the long-term deterioration of surface passivation quality sets in and complicates the analysis.

Interestingly, Hammann et al. [19] investigated the long-term stability of n-type FZ Si wafers subjected to a high-temperature step at 1050 °C in an O_2 atmosphere. During light soaking (75 °C and 1 sun), they observed only an improvement in τ_{eff}. In the fast-cooled sample, a slight change in J_0 was detected, leading the authors to suggest that surface changes had minimal impact on the observed lifetime enhancement. However, under dark annealing, the sample initially showed an improvement in lifetime, followed by degradation. During the initial improvement

phase, the fast-cooled sample exhibited a modest enhancement of 2 fA/cm^2. Thus, the change in surface quality could also affect τ_{eff} in this case.

4 Conclusion

In this work, the influence of high temperature process steps such as tabula rasa (TR) and phosphorous gettering (G) on the long-term stability behavior in *n*-type FZ-Si wafers was investigated. Gettering shows no influence on the long-term stability behavior. The samples that have undergone a TR step show only bulk-related regeneration under LeTID conditions. This behavior could also be observed in darkness, so the effect in general does not seem to be light-induced but charge carrier-induced. FT-IR measurements at 5 K showed that the samples with a TR step have a higher O_i concentration in the Si bulk than the reference samples. This increase in $[O_i]$ can be explained by the dissolution of the silicon oxide agglomerates. In addition, the LVM of VH_4 could not be detected for the samples with a TR step, suggesting that the VH_4 complexes are dissolved by the TR step and do not form again during the firing step when the bulk is flooded with hydrogen. This can be explained by the reduction in vacancy concentration during TR treatment. This observation indicates a possible involvement of the vacancies in the degradation process. The injection-resolved defect densities were examined to analyze the defect during regeneration, revealing that the disappearance of the defect cannot be solely attributed to changes in surface passivation quality, but also involves a bulk-related defect.

While degradation phenomena as well as mitigation strategies are well known for *p*-type Si materials, the detailed investigation on *n*-type Si wafers is a rather new field of research, especially with respect to LeTID. The high-temperature processing steps shown here, such as TR, activate bulk defects, which later disappear during exposure to illumination and/or temperature. Interestingly, the TR treated samples show after regeneration higher τ_{eff} values compared to the reference samples, which started at higher τ_{eff} levels directly after firing. This regeneration was observed in *n*-type FZ material. However, due to significant differences in $[O_i]$ and intrinsic defect concentrations between FZ and Cz Si, these results may not be directly applicable to Cz material.

Acknowledgments

The authors would like to thank Bärbel Rettenmaier for technical support.

Funding

Part of this work was funded by the German Federal Ministry for Economic Affairs and Climate Action (BMWK) under contract number 03EE1176C. The Research Council of Norway is acknowledged for the support of the Norwegian Micro- and Nanofabrication Facility, NorFab, project number 295864. Funding parts of this work was also provided by the Norwegian Research Council through the Research Center for Sustainable Solar Cell Technology (FME SUSOLTECH, No. 257639). The content is the responsibility of the authors.

Conflicts of interest

The authors declare that they have no known competing financial interests or personal relationships that could have appeared to influence the work reported in this paper.

Data availability statement

Data will be made available on request.

Author contribution statement

Melanie Mehler: Writing – review & editing, Writing – Original Draft, Methodology, Investigation, Formal analysis, Conceptualization. **Nicolas Weinert:** Methodology, Investigation, Formal analysis. **Nicole Aßmann:** Writing – review & editing, Methodology, Investigation, Formal analysis. **Axel Herguth:** Writing – review & editing, Validation, Methodology. **Giso Hahn:** Writing – review & editing, Supervision, Resources, Funding acquisition. **Fabian Geml:** Writing – review & editing, Conceptualization, Supervision, Project administration.

References

1. V. LaSalvia, A. Youssef, M.A. Jensen, E.E. Lonney, W. Nemeth, M. Page, W. Nam, T. Buonassi, P. Stradins, Tabula Rasa for *n*-Cz silicon-based photovoltaics, Prog. Photovol.: Res. Appl. **27**, 136 (2019). https://doi.org/10.1002/pip.3068
2. J.M. Hwang, D.K. Schroder, Recombination properties of oxygen-precipitated silicon, J. Appl. Phys. **59**, 2476 (1986). https://doi.org/10.1063/1.336993
3. M. Pagani, R.J. Falster, G.R. Fisher, G.C. Ferrero, M. Olmo, Spatial variations in oxygen precipitation in silicon after high temperature rapid thermal annealing, Appl. Phys. Lett. **70**, 1572 (1997). https://doi.org/10.1063/1.118620
4. J.D. Murphy, R.E. McGuire, K. Bothe, V.V. Voronkov, R.J. Falster, Minority carrier lifetime in silicon photovoltaics: The effect of oxygen precipitation, Sol. Energy Mater. Sol. Cells **120**, 402 (2014). https://doi.org/10.1016/j.solmat.2013.06.018
5. R.J. Falster, M. Cornara, D. Gambaro, M. Olmo, M. Pagani, Effect of high temperature pre-anneal on oxygen precipitates nucleation kinetics, Solid State Phenom. **57**, 123 (1997). https://doi.org/10.4028/www.scientific.net/SSP.57-58.123
6. S.M. Hu, Precipitation of oxygen in silicon: Some phenomena and a nucleation model, J. Appl. Phys. **52**, 3974 (1981). https://doi.org/10.1063/1.329204
7. R. Basnet, F.E. Rougieux, C. Sun, S.P. Phang, C. Samundsett, R. Einhaus, J. Degoulang, D. Macdonald, Methods to improve bulk lifetime in *n*-type Czochralski-grown upgraded metallurgical-grade silicon wafers, IEEE J. Photovolt. **8**, 990 (2018). https://doi.org/10.1109/JPHOTOV.2018.2834944
8. V.V. Voronkov, R. Falster, Vacancy and self-interstitial concentration incorporated into growing silicon crystals, J. Appl. Phys. **86**, 5975 (1999). https://doi.org/10.1063/1.371642
9. V.V. Voronkov, R. Falster, Vacancy-type microdefect formation in Czochralski silicon, J. Cryst. Growth **194**, 76 (1998). https://doi.org/10.1016/S0022-0248(98)00550-8

10. D.A. Antoniadis, Oxidation-induced point-defects in silicon, J. Electrochem. Soc. **129**, 1093 (1982). https://doi.org/10.1149/1.2124034
11. T.Y. Tan, U. Gösele, Growth-kinetics of oxidation-induced stacking-faults in silicon – A new concept, Appl. Phys. Lett. **39**, 86 (1981). https://doi.org/10.1063/1.92526
12. D.F. Downey, M. Farley, K.S. Jones, G. Ryding, *Ion Implantation Technology-92* (Elsevier B.V., North Holland, 1993)
13. M.N. Kham, I. Matko, B. Chenevier, P. Ashburn, Reduced boron diffusion under interstitial injection in fluorine implanted silicon, J. Appl. Phys. **102**, 7 (2007). https://doi.org/10.1063/1.2822465
14. J. Ochoa, V. LaSalvia, P. Stradins, M. Bertoni, Understanding the origin of Tabula Rasa-induced defects in *n*-type Cz c-Si: The case of nitrogen atmosphere, Sol. Energy Mater. Sol. Cells **252**, 112159 (2023). https://doi.org/10.1016/j.solmat.2022.112159
15. F. Kersten, P. Engelhart, H.C. Ploigt, A. Stekolnikov, T. Lindner, F. Stenzel, M. Bartzsch, A. Szpeth, K. Petter, J. Heitmann, J.W. Müller, Degradation of multicrystalline silicon solar cells and modules after illumination at elevated temperature, Sol. Energy Mater. Sol. Cells **142**, 83 (2015). https://doi.org/10.1016/j.solmat.2015.06.015
16. J. Fritz, A. Zuschlag, D. Skorka, A. Schmid, G. Hahn, Impact of temperature and doping on LeTID and regeneration in mc-Si, in *Proceedings of the 33rd European Photovoltaic Solar Energy Conference and Exhibition* (WIP Renewable Energies, München, Germany, 2017), p. 569. https://dx.doi.org/10.4229/EUPVSEC20172017-2AV.1.40
17. F. Kersten, P. Engelhart, H.C. Ploigt, F. Stenzel, K. Petter, T. Lindner, A. Szpeth, M. Bartzsch, A. Stekolnikov, M. Scherff, J. Heitmann, J.W. Müller, A new light induced volume degradation effect of mc-Si solar cells and modules, in *Proceedings of the 31st European Photovoltaic Solar Energy Conference and Exhibition* (WIP Renewable Energies, 2015), p. 1830
18. C. Vargas, K. Kim, G. Coletti, D. Payne, C. Chan, S. Wenham, Z. Hameiri, Influence of silicon nitride and its hydrogen content of carrier-induced degradation in multi-crystalline silicon, in *Proceedings of the 33rd European Photovoltaic Solar Energy Conference and Exhibition* (WIP Renewable Energies, München, Germany, 2017), p. 561
19. B. Hammann, N. Assmann, P.M. Weiser, W. Kwapil, T. Niewelt, F. Schindler, R. Søndenå, E.V. Monakhov, M.C. Schubert, The impact of different hydrogen configurations on light-and elevated-temperature-induced degradation, IEEE J. Photovolt. **13**, 224 (2023). https://doi.org/10.1109/JPHOTOV.2023.3236185
20. A.R. Meyer, P.C. Taylor, V. LaSalvia, X. Wang, W. Nemeth, M. Page, D.L. Young, S. Agarwal, P. Stradins, Atomic structure of defect responsible for light-induced efficiency loss in silicon solar cells in warmer climates, Cell Rep. Phys. Sci. **4**, 101201 (2023). https://doi.org/10.1016/j.xcrp.2022.101201
21. D. Chen, P. Hamer, M. Kim, C. Chan, A.C. Wenham, F. Rougieux, Y. Zhang, M. Abbott, B. Hallam, Hydrogen-induced degradation: Explaining the mechanism behind light- and elevated temperature-induced degradation in *n*- and *p*-type silicon, Sol. Energy Mater. Sol. Cells **207**, 110353 (2020). https://doi.org/10.1016/j.solmat.2019.110353
22. C. Vargas, S. Nie, D. Chen, C. Chan, B. Hallam, G. Coletti, Z. Hameiri, Degradation and recovery of *n*-type multi-crystalline silicon under illuminated and dark annealing conditions at moderate temperatures, IEEE J. Photovolt. **9**, 355 (2018). https://doi.org/10.1109/JPHOTOV.2018.2885711
23. D. Chen, P.G. Hamer, M. Kim, T.H. Fung, G. Bourret-Sicotte, S. Liu, C.E. Chan, A. Cisela, R. Chen, M.D. Abbott, B. Hallam, S.R. Wenham, Hydrogen induced degradation: A possible mechanism for light- and elevated temperature- induced degradation in *n*-type silicon, Sol. Energy Mater. Sol. Cells **185**, 174 (2018). https://doi.org/10.1016/j.solmat.2018.05.034
24. C. Renevier, E. Fourmond, M. Forster, S. Parola, M. Le Coz, E. Picard, Lifetime degradation on *n*-type wafers with boron-diffused and SiO_2/SiN-passivated surface, Energy Proc. **55**, 280 (2014), https://doi.org/10.1016/j.egypro.2014.08.082
25. D. Kang, H.C. Sio, X. Zhang, J. Yang, J. Jin, D. Macdonald, Light and elevated temperature induced degradation in mono-like and float-zone silicon: Correlations to material types, silicon nitride films, and dopant diffusion, IEEE J. Photovolt. **11**, 1167 (2021), https://doi.org/10.1109/JPHOTOV.2021.3082645
26. A. Herguth, On the lifetime-equivalent defect density: Properties, application, and pitfalls, IEEE J. Photovolt. **9**, 1182 (2019). https://doi.org/10.1109/JPHOTOV.2019.2922470
27. A. Herguth, J. Kamphues, On the impact of bulk lifetime on the quantification of recombination at the surface of semiconductors, IEEE J. Photovolt. **13**, 672 (2023). https://doi.org/10.1109/JPHOTOV.2023.3291453
28. P.M. Weiser, E. Monakhov, H. Haug, M.S. Wiig, R. Søndenå, Hydrogen-related defects measured by infrared spectroscopy in multicrystalline silicon wafers throughout an illuminated annealing process, J. Appl. Phys. **127**, 065703 (2020). https://doi.org/10.1063/1.5142476
29. B. Pajot, B. Clerjaud, *Optical absorption of impurities and defects in semiconducting crystals: Electronic absorption of deep centres and vibrational spectra* (Springer Science & Business Media, 2013), Vol. 169. http://dx.doi.org/10.1007/978-3-642-18018-7
30. B.B. Nielsen, L. Hoffmann, M. Budde, SiH stretch modes of hydrogen – vacancy defects in silicon, Mater. Sci. Eng. B **36**, 259 (1996). https://doi.org/10.1016/0921-5107(95)01260-5
31. P. Deák, M. Heinrich, L.C. Snyder, J.W. Corbett, Hydrogen-related vibrations in crystalline silicon, Mater. Sci. Eng. B **4**, 57 (1989). https://doi.org/10.1016/0921-5107(89)90216-X
32. F.A. Reboredo, M. Ferconi, S.T. Pantelides, Theory of the nucleation, growth, and structure of hydrogen-induced extended defects in silicon, Phys. Rev. Lett. **82**, 4870 (1999). https://doi.org/10.1103/PhysRevLett.82.4870
33. M. Suezawa, Hydrogen-point defect complexes in electron-irradiated C-doped and high-purity Si, Jpn. J. Appl. Phys. **38**, L608 (1999). https://doi.org/10.1143/JJAP.38.L608
34. P. Bech, B. Nielsen, L. Hoffmann, M. Budde, R. Jones, J.P. Goss, S. Öberg, H interacting with intrinsic defects in Si, Mater. Sci. Forum **196**, 933 (1995). https://doi.org/10.4028/www.scientific.net/MSF.196-201.933
35. E.V. Lavrov, J. Weber, L. Huang, B.B. Nielsen, Vacancy-hydrogen defects in silicon studied by Raman spectroscopy, Phys. Rev. B **64**, 035204 (2001). https://doi.org/10.1103/PhysRevB.64.035204

36. H. Zimmermann, U. Gösele, M. Seilenthal, P. Eichinger, Vacancy concentration wafer mapping in silicon, J. Cryst. Growth **129**, 582 (1993). https://doi.org/10.1016/0022-0248(93)90494-H
37. A.R. Meyer, V. LaSalvia, W. Nemeth, W. Xu, M. Page, D.L. Young, S. Agarwal, P. Stradins, Influence of tabula rasa on process-and light-induced degradation of solar cells fabricated from Czochralski silicon, IEEE J. Photovolt. **10**, 1557 (2020). https://doi.org/10.1109/JPHOTOV.2020.3020214
38. M. Mehler, N. Weinert, N. Aßmann, A. Herguth, G. Hahn, F. Geml, Long-term lifetime instabilities in *n*-type FZ- and Cz-silicon wafers under illumination at elevated temperature, Sol. Energy Mater. Sol. Cells **278**, 113169 (2024). https://doi.org/10.1016/j.solmat.2024.113169
39. T. Niewelt, R. Post, F. Schindler, W. Kwapil, M.C. Schubert, Investigation of LeTID where we can control it-Application of FZ silicon for defect studies, AIP Conf. Proc. **2147**, 140006-1 (2019). https://doi.org/10.1063/1.5123893
40. A. Kimmerle, J. Greulich, A. Wolf, Carrier-diffusion corrected J0-analysis of charge carrier lifetime measurements for increased consistency, Sol. Energy Mater. Sol. Cells **142**, 116 (2015). https://doi.org/10.1016/j.solmat.2015.06.043
41. S. Bernardini, T.U. Nærland, A.L. Blum, G. Coletti, M.I. Bertoni, Unraveling bulk defects in high-quality c-Si material via TIDLS, Prog. Photovolt.: Res. Appl. **25**, 209 (2017). https://doi.org/10.1002/pip.2847

Cite this article as: Melanie Mehler, Nicolas Weinert, Nicole Aßmann, Axel Herguth, Giso Hahn, Fabian Geml, Impact of high-temperature processing steps on the long-term stability of charge carrier lifetime in *n*-type FZ-silicon, EPJ Photovoltaics **16**, 15 (2025), https://doi.org/10.1051/epjpv/2025006